Lab on a Chip

PAPER

View Article Online
View Journal | View Issue

Cite this: *Lab Chip*, 2025, **25**, 1831

A microfluidic twin islets-on-chip device for on-line electrophysiological monitoring†

Marie Lallouet,[a] Loic Olçomendy,[b] Julien Gaitan,[a] Killian Montiège,[b] Marie Monchablon,[ab] Antoine Pirog,[c] Dorian Chapeau,[a] Emilie Puginier,[a] Sylvie Renaud,[b] Matthieu Raoux[a] and Jochen Lang*[a]

Pancreatic islets play a major role in glucose homeostasis as well as in diabetes, and islets-on-chip devices have been mainly developed using optical means for on-line monitoring. In contrast, no well-characterized electrophysiological platform for on-line analysis with unrivalled temporal resolution has been reported. Extracellular electrophysiology monitors two crucial parameters, islet β-cell activity and β-to-β-cell coupling, does not require chemical or genetic probes with inherent potential bias, is non-invasive and permits repetitive long-term monitoring. We have now developed and characterized a microfluidic islets-on-chip for combined electrophysiology (on-line) and hormone monitoring (off-line) with two chambers for concomitant monitoring. Fabrication of the device, based on commercial or easily manufacturable components, is within the reach of non-specialized laboratories. The chip permits convenient loading as well as long-term culture with comparable glucose kinetics and low shear stress in both chambers. An optimized flow rate did not alter islet β-cell electrical activity or coupling in response to glucose. Culturing for up to 8 days did not change islet survival as well as glucose-induced electrical or secretory kinetics of islet β-cells. The addition of a physiological amino acid mix, in the presence of elevated glucose, made a considerable change in the functional organisation of islet β-cell activity in terms of frequency and coupling, which explains the ensuing strong increase in insulin secretion. This device thus allows reliable long-term multiparametric on-line monitoring in two islet populations. The ease of fabrication, assembly and handling should permit widespread long-term on-line monitoring of islet activity in native micro-organs (*e.g.* controls/mutants), pseudo-islets or stem-cell-derived islet-like organoids.

Received 17th November 2024,
Accepted 2nd February 2025

DOI: 10.1039/d4lc00967c

rsc.li/loc

1. Introduction

Diabetes is an increasingly prevalent, chronic and incurable disease, characterised by elevated blood glucose levels.[1] In its most prevalent form, type 2 diabetes, pancreatic β-cell dysfunction plays a crucial role.[2] For this reason, the study of β-cells has focused on islet function in physiological and dynamic microenvironments.[3]

Pancreatic islets contain four main cell types, β, α, δ and γ cells, which secrete insulin, glucagon, somatostatin or pancreatic polypeptide, respectively.[4] Islet cells are electrogenic, and in the case of β-cell response to an increase in glucose, their metabolism augments the ATP/ADP ratio, and the ensuing closure of K_{ATP} channels results in plasma membrane depolarisation, opening of voltage-dependent Ca^{2+}-channels and exocytosis of insulin *via* a Ca^{2+}-dependent process.[5] Activation of islets by glucose leads to a typical biphasic response, with a marked, short-lasting first phase and a longer, less pronounced second phase. A normal diet also contains amino acids, which make up about a quarter of the recommended dietary caloric intake, but amino acids are less often considered in regard to β-cell responses *in vitro*.[6]

To study islet and β-cell function, a number of islet(s)-on-chip devices have been published as culture and analysis platforms over the two past decades,[3] ranging from simple single-channel or compartment devices for mass analysis[7–9] to sophisticated models for single-islet analysis,[10–12] linking islets with other organoids-on-chips,[13,14] obtaining vascularised islets[15,16] or featuring on-line determination of hormones and other secreted molecules of physiological relevance.[17–19] In most instances, islet activity has been determined *via* on-line fluorescent measurements of calcium or redox intermediates[12,20–22] or analysis of hormone secretions.[17,23–25]

The monitoring of cell, organoid or micro-organ activity by extracellular electrophysiology offers certain advantages

[a] *Univ. Bordeaux, CNRS, Bordeaux INP, Institute of Chemistry and Biology of Membranes, CBMN, UMR 5248, Pessac, France. E-mail: jochen.lang@u-bordeaux.fr*
[b] *Univ. Bordeaux, CNRS, Bordeaux INP, Integration from Material to System, IMS, UMR 5218, F-33400 Talence, France*
[c] *Junia, Electronics-Physics-Acoustics Department, F-59000 Lille, France*

† Electronic supplementary information (ESI) available. See DOI: https://doi.org/10.1039/d4lc00967c

compared to other currently used approaches.[26,27] Extracellular electrophysiology is on-line and non-invasive, ensuring long-term survival of the sample. It does not require loading with fluorescent agents, which precludes long-term studies, or genetic manipulation of the biological sample (*e.g.* genetically encoded sensors) with evident problems of potential bias or, as in the case of viral transduction, of variable penetration into the whole islet. In addition, the chip and its biological sample are reusable, allowing comparisons over time. Moreover, electrophysiology offers a temporal resolution unmatched by other methods and is compatible with real-time electronic processing.[9,28] Most early microfluidic electrophysiology was done in neurons or cardiomyocytes,[29,30] as those cells depolarize to much larger positive voltages than pancreatic islet cells[5] and consequently those recordings are less sensitive to noise. Extracellular electrophysiology by microelectrode arrays MEAs or organic–electrochemical transistors of islets measures changes in field potentials and thus allows the detection of single cell events *via* the frequency of slow potentials.[31,32] In addition to β-cells, δ-cells may contribute to electrical signals but are numerically only minor components of islets[33] whereas α-cells are never detected.[34] Furthermore, intercellular coupling and coordination between islet β-cells are hallmarks of islet activation,[35] which can be reliably detected and analysed without bias by monitoring the amplitude of so-called slow potentials.[7,31,34,36] In β-cells, the main ionic current is caused by Ca^{2+} fluxes,[37] and signals recorded by MEAs are closely linked to insulin secretion driven by calcium influx,[7] providing insights at the millisecond scale. Finally, MEAs or other electrodes and transistors[31] are open to future development for on-line detection of specific compounds, such as Zn^{2+}, as surrogates for insulin secretion.[38–40]

We have now developed an on-line electrophysiological microfluidic chip for pancreatic islets coupled to off-line measurements of insulin secretion with certain characteristics. In-house fabrication of MEAs is intensive work and requires a considerable degree of skill and amount of equipment, and often exhibits an unfavourable signal/noise ratio,[26,41] while high-quality MEAs are commercially available. Adapting the microfluidic chip to existing commercial MEA layouts should ensure high-quality recordings and general accessibility for non-specialized laboratories. Electrophysiological recordings require electrode–islet contact and thus preclude certain very elegant chip configurations in PDMS,[10] except when resorting to complex and expensive procedures such as micromilling.[42] In the same vein, fabrication of the chip should be easy, to permit its widespread use. A system with at least two (islet) channels offers the advantage of comparing distinct samples (*e.g.* control and mutant) within the same experiment. The device should permit easy sample loading and long-term culture. Moreover, the chip should also monitor more than one physiological parameter. As fully translucent electrodes are not yet available in MEAs,[42] fluorescent imaging is not an option, but the concomitant collection of fractions for hormone assays should be included, despite the risk of increasing noise in MEA recordings.

2. Material and methods

2.1. Materials

All chemicals were purchased from Sigma-Aldrich (St. Louis, MO, USA). Thapsigargin and forskolin were dissolved in dimethyl sulfoxide (final concentrations ≤0.1%, vol./vol.).

2.2. Microfluidic chip design

The microfluidic chip mold and caps were drawn using Fusion 360 software (Autodesk, San Francisco, CA, USA) prior to 3D printing by stereolithography with ABS-like resins. The mold was fabricated by ProtoLabs using MicroFine resin (Proto Labs, Le Bourget du Lac, France). Caps were produced using an LCD 3D printer (ELEGOO, Mars 2, Lespinasse, France). Caps were washed with isopropyl alcohol, UV-cured for 12 hours, further cured at 60 °C for 6 h and sterilised with 70% ethanol. The microfluidic chip was fabricated using polydimethylsiloxane (PDMS). PDMS was poured onto the 3D mold without covering the chambers and polymerised at room temperature for 48 h. The microfluidic chip on MEA (μMEA) was obtained by bonding PDMS chips onto MEA500/30iR-Ti-gr (electrodes with 30 μm of diameter are spaced 500 μm apart, Multi Channel Systems MCS, Reutlingen, Germany) using surface activation by oxygen plasma (RIE FLIRE300 C, Diener Electronic, Ebhausen, Germany). A ring (Ø 1 mm, h = 12 mm) was printed by the fused deposition modelling method[43] and bonded to μMEA with unpolymerized PDMS at 60 °C for 3 hours.

2.3. Microfluidic system

Fig. 1A shows the experimental setup. The flow was driven by a vacuum pump (MFCSEZ; Fluigent, Villejuif, France), split between up to 10 tubes (Falcon, Thermo Fisher, Illkirch Graffenstaden, France) and maintained at 37 °C. A distributor valve automatically selected the solution to be injected into the chip (M-Switch; Fluigent, Villejuif, France). The flow rate was controlled by a flow sensor (Flow unit M; Fluigent, Villejuif, France) operating at up to 120 μl min^{-1}. The outlet was connected to a microfraction collector (Amuza Inc., FC-90, San Diego, California) with a 96-well plate pre-coated with BSA 0.1%. PFTE tubing was used along with high-resistance PEEK tubing to achieve a minimum pressure of more than 100 mbar for flow stability. The inlet and outlet flow were connected to the electrical ground by steel tubes. All devices were monitored automatically using pre-programmed protocols *via* Microfluidic Automation Tool (MAT) software for the Fluigent devices and Amuza software for the fraction collector. All equipment was carefully earthed to reduce electrical noise.

2.4. Simulations

The entire experimental microfluidic setup (including tubing and fraction collector) was modelled in COMSOL Multiphysics software 6.1 (COMSOL Inc., Burlington, MA, USA) to generate a digital twin of the setup, to simulate the

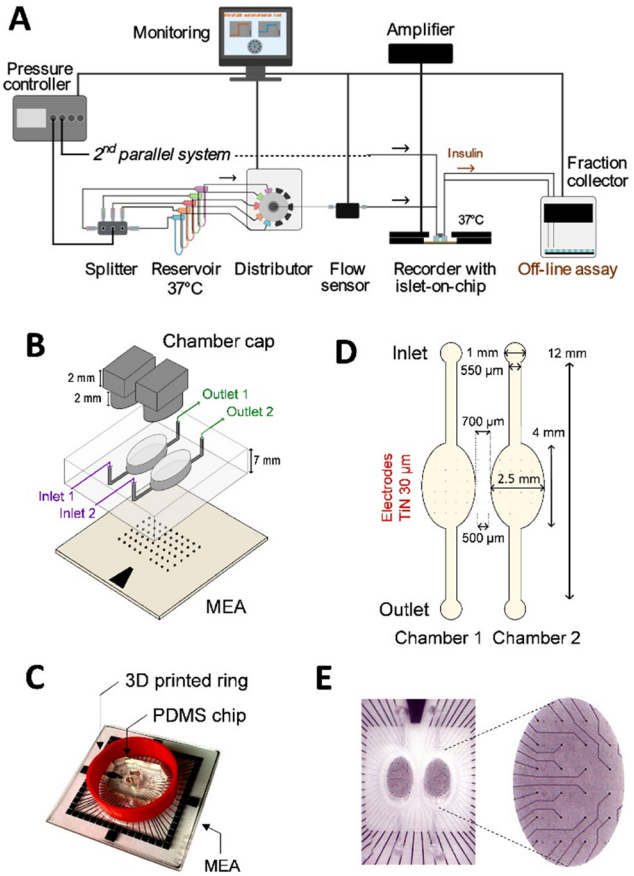

Fig. 1 Overview of the microfluidic system and of the design of the islets-on-chip. (A) Front view of the automated microfluidic MEA system and fraction collector. (B) Exploded view of the microfluidic chip. PDMS chambers are bonded to the MEA by O_2 plasma and closed with 3D-printed caps. The reference electrode is given in black. (C) Image of the assembled microfluidic chip with 3D-printed media containment ring. (D) Drawing of the channels and chambers on the electrodes and corresponding dimensions. The TiN electrodes (Ø 30 µm) were spaced 500 µm apart. (E) Image of the chambers with the electrodes in titanium nitride (TiN).

circulation of chemical species within the chamber up to the collector. Two physics interfaces were used: "laminar flow" to compute the pressure and fluid velocity dynamics within the microfluidic setup, and "transport of diluted species" to compute the resulting variations in concentration of chemical species. Physical parameters were set according to the literature: the diffusion rate of glucose was 8.5×10^{-10} m^2 s^{-1} and the dynamic viscosity of water (at 37 °C) was μ = 6.913×10^{-4} Pa s.[25,44,45] All the tubing dimensions, from the distributor to the fraction collector, were duplicated to the experimental dimensions. Simulations were performed with a hybrid 2D axisymmetric/3D model. As the velocity gradient of a fluid flowing in a cylinder presents a concentric shape, the tubing was modelled as a 2D-axisymetric cylinder coupled to a 3D model of the microfluidic chamber, to decrease simulation time. For each *in vitro* experiment, the experimental protocol was accurately reproduced *in silico*, in terms of flow rate, concentration of studied species, and duration. The simulation validation was performed with a colorimetric glucose assay (Thermo Fisher, Illkirchen Graffenstaden, France).

2.5. Assessment of islet viability and activity

Adult male C57BL/6J mice (12–22 weeks old) were sacrificed by cervical dislocation, according to the University of Bordeaux ethics committee guidelines. Islets were obtained by enzymatic digestion and hand-picking and cultured for 12 hours at 37 °C (5% CO_2, 90% relative humidity) in RPMI medium (11 mmol l^{-1} glucose, Thermo Fisher, Illkirchen Graffenstaden, France).[7,36,46] The microfluidic chip was cleaned and hydrophilized by air plasma (Diener Electronic, Ebhausen, Germany) for 2 minutes and loaded with Matrigel (5% v/v) (BD Biosciences, San Diego, CA), at room temperature for 30 minutes.[7,32,47] Between 150 and 200 islets were loaded through the top of the chamber with culture medium to achieve a final Matrigel concentration of 2% (v/v). After 45 minutes, culture medium was added and the chip was stored at 37 °C (5% CO_2, 90% relative humidity). The medium was changed every 3 days.

Islet viability was assessed using a LIVE/DEAD kit assay (Thermo Fisher, Illkirchen Graffenstaden, France) 4 and 8 days after seeding. Half of the culture medium was removed and the same volume of calcein AM and ethidium homodimer-1 were added to the chambers for at least 90 min at room temperature. Images were taken at 494/517 nm (excitation/emission) for live cells and 528/617 nm (excitation/emission) for dead cells. Hypoxia was detected using a fluorescent marker (BioTracker 520 Green Hypoxia Reagent) according the manufacturer's instructions.

Insulin secretion was collected every 2 min in BSA-coated plates, stored at −20 °C and quantified using mouse insulin ELISA kits (Mercodia, Uppsala, Sweden).

2.6. Electrophysiology

Experiments in µMEA chips were performed at 37 °C in a buffer containing (in mM) NaCl 135, KCl 4.8, $MgCl_2$ 1.2, $CaCl_2$ 1.2, HEPES 10 and glucose and amino acids as indicated (pH 7.4 adjusted with NaOH). The physiological amino acid mix was prepared as follows: Ala 0.88, Arg 0.38, Asp 0.076, Cit 0.19, Glut 0.24, Gly 0.6, His 0.15, Ile 0.19, Leu 0.32, Lys 0.74, Met 0.1, Orn 1.4, Phe 0.16, Pro 0.7, Ser 1.14, Thre 0.54, Trp 0.15, Val 0.4, Glut 2 (in mM).[48] Extracellular recordings were performed on the µMEA placed in an MEA recording system (MEA1060 System, Multi-Channel Systems GmbH [MCS], Reutlingen, Germany). Extracellular field potentials were acquired at 10 kHz, amplified, and band-pass filtered at 0.1–3000 Hz using a USB-MEA60-Inv-System-E amplifier (MCS; gain: 1200) controlled by MC_Rack software (v4.6.2, MCS).[7,36,46] Images of islets on MEAs were taken before and after each experiment to localize electrodes covered with islets. Electrophysiological data were analysed with MC_Rack software. Slow potentials (SPs) were isolated using a 0.1–2 Hz band-pass filter, and frequencies were

determined using the threshold module of MC_Rack with a dead time (minimum time between two events) of 300 ms (SPs). The peak-to-peak amplitude module of MC_Rack was used to determine SP amplitudes.[7,36,46]

2.7. Statistics

Graphics, quantifications, and statistics were performed with Prism software (v7; GraphPad, La Jolla, CA). Data are presented as means and SEM. The minimal value of mean SP frequency after the first peak (corresponding to the lowest point) was taken as the limit between phases. Gaussian distributions were tested using the Shapiro–Wilk test and comparison of two groups with paired data by two-tailed unpaired *t*-tests or nonparametric Mann–Whitney tests. For more than two groups, one-way ANOVA with appropriate *post hoc* tests was used, as indicated in the legends.

3. Results

3.1. Microfluidic system and islet-on-chip design and fabrication

The first aim was to design an automated microfluidic system, optimised for extracellular MEA recording of a standardised microfluidic islets-on-chip (Fig. 1). The system required easy access to culture medium, islet loading and contact of islets to the microelectrodes of the MEA. Moreover, it had to be compatible with commercial MEAs which have an excellent signal/noise ratio. The choice of equipment was further guided by the sensitivity of electrophysiological measurements to flow fluctuations, which introduce noise that interferes with optimal measurement of electrical islet signals. Consequently, the microfluidic system consisted of a pump, a pressure controller and a flow sensor to control the flow either by pressure or flow rate (Fig. 1A).

The use of a splitter and a distributor allows the injection of up to 10 different solutions each kept at 37 °C. The length and diameter of the tubing were chosen to ensure pressure above 100 mbar for a stable flow rate. The liquid inside the tubes upstream and downstream of the chip and all the equipment were electrically earthed (Fig. 1A). All microfluidic devices were automatically controlled by software (fluids, MAT; MEA, MC_Rack v4.6.2; fraction collector, FC-90 Amuza apps *via* Bluetooth) according to previously established protocols.[7,9] For electrophysiological measurements, the microfluidic chip was inserted into the temperature-controlled MEA-System, which amplified and recorded the signals detected by the electrodes. The outlet of the chip was connected to an automated fraction collector.

The chip itself consisted of two parallel open PDMS chambers bonded to an MEA (Fig. 1B). A 3D-printed ring was added to encircle the PDMS chambers and maintain a large volume of medium during islet culture (Fig. 1C). The chambers were open for loading of islets and culture and closed with 3D-printed caps during the fluidic experiments. In terms of dimensions, the commercial MEAs were chosen with 500 μm electrode spacing to distribute microelectrodes throughout the chamber (Fig. 1D and E). The chamber dimensions were optimised according to three criteria: (i) the distribution of the electrodes within the chambers, (ii) the distance between the two chambers to ensure bonding of the PDMS wall separating them (≥0.5 mm), and (iii) the flow in terms of shear stress and kinetics of changes in glucose concentrations.

3.2. Model validation in COMSOL for characterisation of microfluidic flow in the twin chambers

COMSOL Multiphysics simulation software was used to visualise the fluid circulation inside the chip and optimise the microfluidic system. The tubing and its dimensions were designed in COMSOL based on the experimental setup (Table S1†).

Glucose kinetics for a step from 3 to 11 mM of glucose were simulated and glucose was measured at different points in the system (Fig. S1A†). A delay of 136 s was found for the solution to reach the chip without altering its square pulse kinetics profile (blue line). The squared profile in glucose ascent and descent was slightly smoothed by the flow transition through the chip (red line). A glucose diffusion phenomenon was observed inside the downstream tubing. A short delay was evident between the plateau of the glucose injected (chip inlet) and the glucose collected (chip outlet), not considering the 3 min delay due to the circulation in the tubing (collector). The tubing between the chip and the fraction collector added only a slight delay during the ascent or descent of glucose, which is easily explained. Subsequently, the simulation of the complete system was compared with the direct experimental determination of glucose concentrations in the absence of islets (Fig. S1B†). Switching glucose solutions from 3 to 11 mM, the stimulatory glucose level of 5 mM was reached after 1.5 min and the maximal value of 11 mM was attained after 5 min of switching. The two chambers (Fig. S1B†) showed very similar kinetics and very good agreement with the simulation, which thus validates the simulation model.

3.3. Optimisation of flow parameters for islets activity measurement

To estimate the effect of chip geometry and flow rate on shear stress, shear stress was determined at flow rates from 15 to 100 μL min^{-1} (Fig. 2A and B). As expected, shear stress was highest at the inlet and the outlet of the chip. At 70 and 100 μL min^{-1}, shear stress values approached the limit of 6 mPa for electrodes in these areas, but remained low (<1 mPa) for two-thirds of the electrodes. Interestingly, at 50 μl min^{-1} or lower, this value was below 4 mPa for all the electrodes in the chamber.

A comparison of the glucose kinetics between 3 and 11 mM was simulated for increasing and decreasing concentrations between 15 and 50 μL min^{-1} at the electrodes (Fig. 2C and D) and at the collector (Fig. 2E). Note that mouse β-cell electrical activity starts to increase from a threshold at

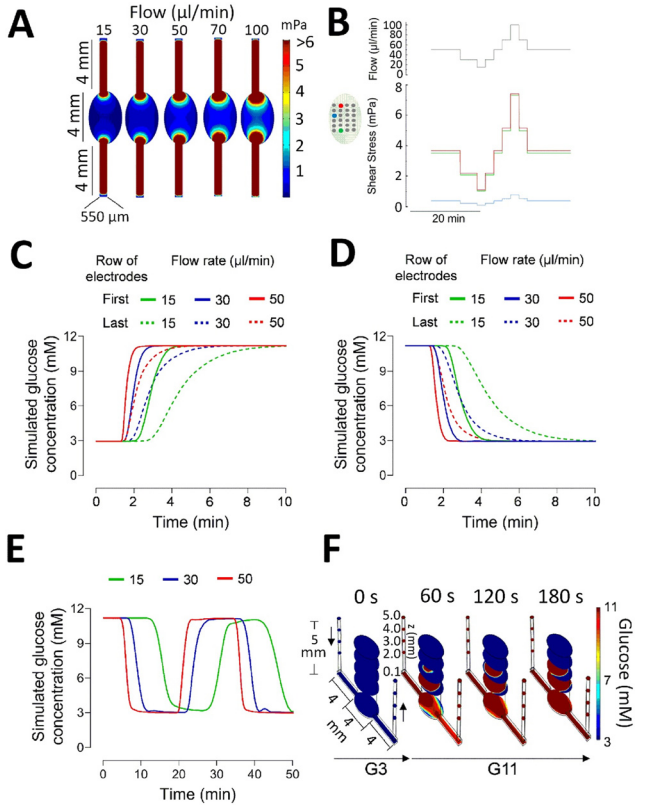

Fig. 2 Optimisation of flow rate for islet activity measurement. (A) Simulated shear stress at the electrode (bottom) level at different flow rates (15 to 100 µl min^{-1}); dimensions of channels and chamber are given. (B) Simulated shear stress as measured over three distinct electrodes either at the entry/exit (red, green) or at the middle border (blue) under indicated flow rates. (C) Simulated glucose concentrations during an increase from 3 to 11 mM glucose or (D) decrease from 11 to 3 mM glucose on the first or last row of electrodes (full *vs.* dashed lines) in the chamber using a flow of 15 (green), 30 (blue) and 50 µl min^{-1} (red). (E) Simulated glucose concentrations at the fraction collector at different flow rates. (F) 3D presentation of changes in glucose concentrations over the whole 5 mm deep chamber (after closure by caps; islets are at the bottom; *z*-planes are indicated) at a flow rate of 50 µl min^{-1}.

6 mM,[7,9] and a range of glucose concentrations between 8.2 and 11 mM is commonly used to simulate postprandial glucose concentrations. At 15 µL min^{-1}, a 72 s delay was found between the first and the last row of electrodes to cross the 6 mM threshold of glucose concentration (Fig. 2C). As expected, doubling the flow rate halved these times between the first and the last rows of electrodes. Increasing the flow rate to 50 µL min^{-1} further reduced this delay time. In this case, starting from 3 mM glucose, a delay of 20 s was observed to reach 6 mM of glucose in the last row of electrodes compared to the first row, 34 seconds to reach 8.2 mM, and 64 s to reach 11 mM. Symmetrical behaviour was observed when the glucose concentration was decreased from 11 to 3 mM (Fig. 2D). The flow rate influenced the diffusion in the downstream tubing to the collector (Fig. 2E), which has been taken into consideration during the subsequent analysis of secretion data. A 3D view of the glucose concentrations at 50 µL min^{-1} is given in Fig. 2F, indicating a rather homogenous distribution in the bottom part of the chamber, *i.e.* the plane of the electrodes and islets. The bottom part of the 5 mm deep chambers changes glucose concentrations according to input concentrations, whereas the concentration in the upper part is not altered. Determination of glucose at the outlet of the chip in the presence of islets confirmed the simulation values, suggesting the absence of any significant changes in glucose concentrations by islet metabolism (Fig. S2†). We chose 50 µL min^{-1} as the flow rate, as it results in a negligible delay in the activation and deactivation of β-cell activity between all the electrodes and negligible shear stress.

3.4. Measurement of β-cell electrical and secretory activity

Nutrient metabolism in islet β-cells leads *via* numerous steps to the opening of voltage-gated channels and insulin secretion (Fig. 3A).[5] MEAs measure changes in field potentials due to ionic currents emitted by channels near electrodes and we have coupled this approach to hormone measurement, such as insulin, in the fractionated effluent with an ELISA off-line assay (Fig. 3A). As these biological parameters depend strongly on the viability of the islets and their adhesion to the electrodes, the seeding protocol was optimised for the microfluidic device (Fig. 3B). Small and medium-sized islets (<100 µm) were selected and seeded in the microfluidic chamber coated with polymerised extracellular matrix, *i.e.* Matrigel. The islets were placed homogeneously throughout the chamber to allow optimal coverage of the electrodes without aggregation of the islets. After 4 days of culturing, half of the electrodes were covered by islets in each chamber (Fig. 3B). Electrodes without islets were used as quality and noise control in the analysis.

To evaluate the impact of flow rates on electrical islet activity, the chip was perfused at low (3 mM) and elevated (11 mM) glucose (Fig. 3C). The latter concentration was chosen as at lower glucose concentrations, pancreatic islets showed physiological electrical oscillations starting about 40 min after the glucose increase, which complicates the analysis.[7] Glucose stimulation induced a clear biphasic response, a hallmark of β-cell activity,[5] with a short first phase and a long-lasting second phase (Fig. 3D). The flow rate was changed during the stimulation with 11 mM glucose (Fig. 3C and D), when the signal reached the plateau of the second phase as a steady state (without oscillations and silent periods). Comparable kinetics of electrical activity were found between the two chambers in culture medium, at low glucose and high glucose for the first and second phases and also in response to forskolin, an activator of adenylyl cyclases. A tendency to changes in mean SP frequencies and amplitudes at 11 mM glucose was found for flow rates above 50 µL min^{-1}, though they were not statistically significant (Fig. 3E and F).

The analysis of the mean SP frequency and amplitude confirmed that the different stimulations induced significant

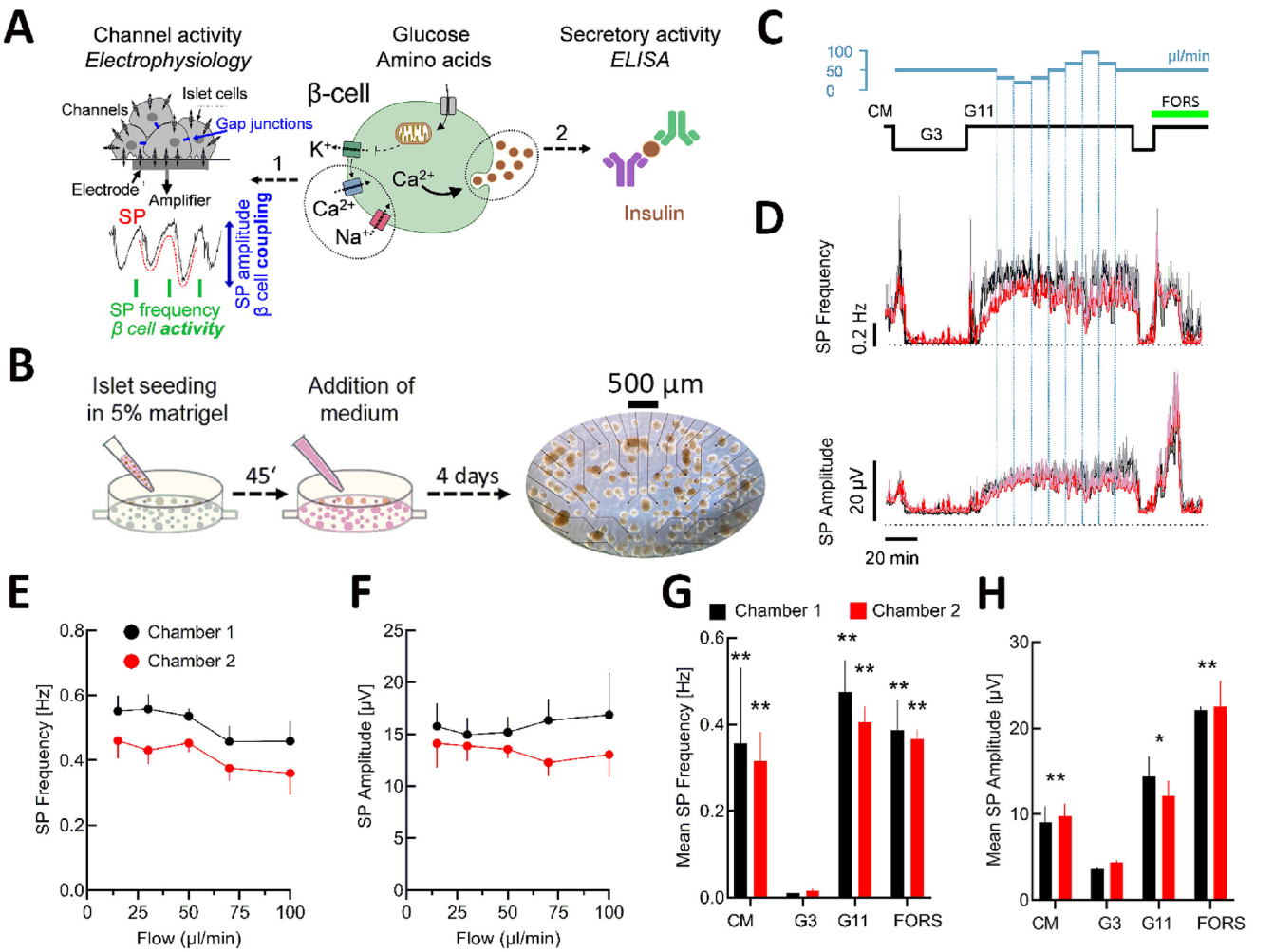

Fig. 3 Characterisation of islet β-cell activity on the microfluidic chip. (A) Scheme of β-cell activation in response to nutrients flanked by the methods used to determine electrical and secretory activity (extracellular electrophysiology on MEAs for on-line detection of slow potentials, SPs, and determination of insulin secretion off-line by ELISA). On the left, a magnification of islet cells on an electrode, measuring and amplifying the β-cell specific slow potential signals (SP, in red). On the right, the measurement of insulin secretion by ELISA assay. (B) Seeding and culture of pancreatic islets on the microfluidic MEA; an image of the entire culture/recording chamber is given on the left with electrodes (black dots), islets (brownish circular structures) and scale bar. (C) Solution and flow rates used during experiments. (D) Recording of slow potentials in complete medium (CM), 3 mM glucose (G3) and at 11 mM (G11) glucose under different flow rates for chamber 1 (black) and chamber 2 (red). SP frequencies and SP amplitudes (mean ± SEM), n = 8–11 are given. SEM is given in grey or light red. (E) and (F) are mean SP frequencies and amplitudes for both chambers at different flow rates, n = 8–11. (G) and (H) Overall effect of complete medium (CM), 3 or 11 mM glucose (G3, G11) and the adenylyl cyclase activator forskolin (FORS, 10 µM) on mean SP frequency and amplitude (mean ± SEM), n = 8–11; *, **, *** $2p < 0.05$, 0.01 or 0.001 (ANOVA/Dunnett) *versus* G3.

changes in electrical islet activity (Fig. 3G and H). Moreover, we did not see any significant difference between their effects in chamber 1 *versus* chamber 2. We also noticed an improvement in performance in terms of pressure effects and electrode distribution compared to our initial chip design (Fig. S3†). Collectively these data validate the physical parameters and the comparability between the two chambers in the chip.

3.5. Long-term culture and analysis

In view of long-term and repetitive measurements, we tested the activity of the islets after 4 and 8 days of culturing in our microfluidic system (Fig. 4). First, we examined the conditions for islet cell survival and hypoxia, the latter being a recurrent problem in suspension cultures.[49] The survival of the islets on the microfluidic chips was tested after 4 and 8 days of culturing on the chip, and representative images of islets on an electrode are shown in Fig. 4A. Only a few dead cells were found after 4 and 8 days of culturing, whereas the addition of 1 µM of thapsigargin for 6 h used as a positive control induced a considerable amount of cell death, as expected. The fluorescent oxygen probe showed no hypoxia after 8 days in culture, in contrast to islets that remained in suspension (Fig. 4B).

The electrical and secretory activity of β-cells was tested during the same culture period after 4 and 8 days and both

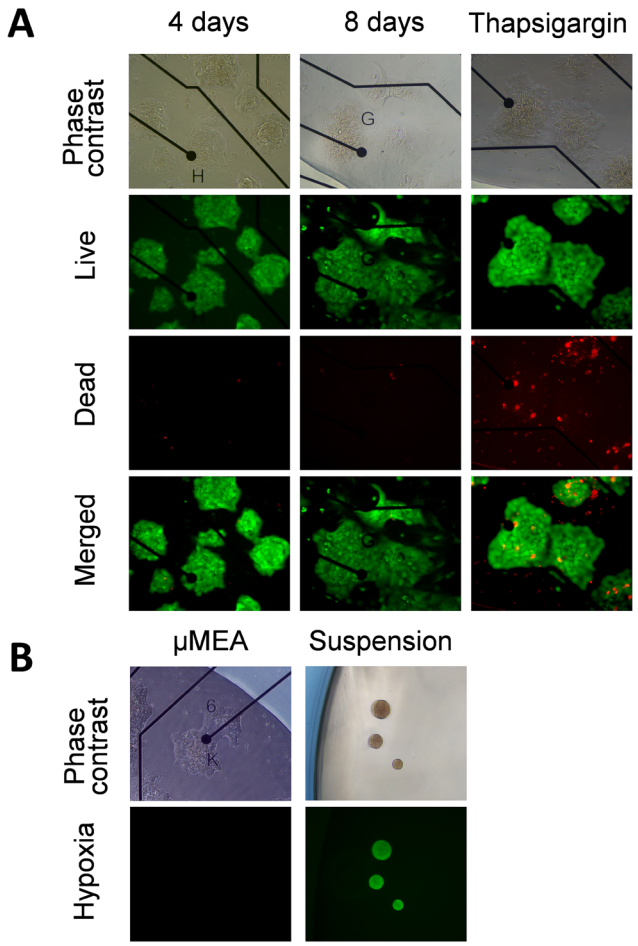

Fig. 4 Long-term islet cell viability on the microfluidic chip. (A) Representative live/dead images of mouse islets on electrodes (green, calcein, live; red, ethidium homodimer, dead) under normal conditions after either 4 or 8 days of culturing or after exposure to apoptosis-promoting tharpsigargin (1 μM, 6 h) at day 8. (B) Comparison of intra-islet oxygen of islets either cultured on the microfluidic MEA Chip (μMEA) or in suspension (suspension). Staining with BioTracker 520 Green Hypoxia Reagent identifies hypoxic cells (green).

microfluidic chambers were compared (Fig. 5). Analysis of signal/noise ratios (Fig. S5†) showed values similar to those we published before[7] despite the fact that additional components (fraction collector) were coupled to the device. As given in Fig. 5A, 11 mM glucose induced an increase in frequency and amplitude with a clear first and second phase. Frequencies and insulin secretions remained comparable between the chambers and days of culturing, whereas a difference was apparent in absolute values of amplitudes between the chambers at day 4, but not at day 8. In contrast to frequency, amplitude is influenced by islet adhesion and the degree of covering a given electrode. Normalisation of recorded amplitudes (Fig. S4†) revealed comparable kinetics between the two chambers. The adenylyl cyclase activator forskolin, added only on day 8 as it may alter subsequent islet function, induced similar changes for both parameters in the chambers.

Glucose at 11 mM induced a typical biphasic pattern with a first phase and second phase in electrical responses and in insulin secretion (Fig. 5A and B). The changes were quantified (Fig. 5C and D) and were most often significant. The addition of amino acids, in the presence of 11 mM glucose during the second phase, produced a remarkable effect (Fig. 5B and D): an increase in frequency and initially a strong decrease in amplitude. During the decrease in amplitude a steep and large increase in insulin secretion was observed. Statistical analysis centred on the effect of amino acids on slow potential frequency, amplitude and insulin secretion 6 min before and after their addition is given in Fig. S6.† The addition of forskolin at the end of the experiments increased insulin secretion, similar to its effect on the frequency and amplitude of SPs (Fig. 5A and B).

4. Discussion

We have developed here a microfluidic two-chamber device for pancreatic islet electrophysiology. Its detailed simulation and characterisation indicated comparable flow parameters in both chambers as well as functional behaviour of mouse islets. Although microfluidics have been used for islets for two decades,[17] only one electrophysiological system had been published, by our group, which, however, did not allow precise kinetics, was not characterized for flow kinetics,[9] was not coupled to a hormone secretion assay, and was designed only for acute experiments, *i.e.* several hours after seeding. To permit more widespread use of microfluidic electrophysiology in laboratories without access to material science, our device now relies on a combination of commercially available components, unlike our previous work.

The use of the device also provided new biological insights. Amino acids are part of a normal diet and are known to stimulate islets,[50] and consequently insulin secretion.[48,51] Here they had an interesting effect on the electrical activity of islet β-cells by immediately increasing SP frequency and insulin secretion but strongly reducing SP amplitude. We have previously shown that the two known phases of islet activation have distinct electrophysiological profiles in extracellular recordings.[7] The first phase, characterized by its strong but short-lived insulin secretion, has high SP frequency but relatively low SP amplitude, reflecting highly active but poorly coordinated islet β-cells. In contrast, the second phase, characterized by moderate but long-lasting hormone release, exhibits lower SP frequency and higher SP amplitude, reflecting highly synchronized islet β-cells working in an energy-sparing mode. Modelling revealed that SP frequency is positively correlated with insulin secretion, whereas amplitudes are negatively correlated. Thus, the electrical pattern observed here suggests that amino acids, in the presence of elevated glucose, lead to a functional reorganisation of electrical islet β-cell networks, resulting in a considerable surge in insulin secretion.

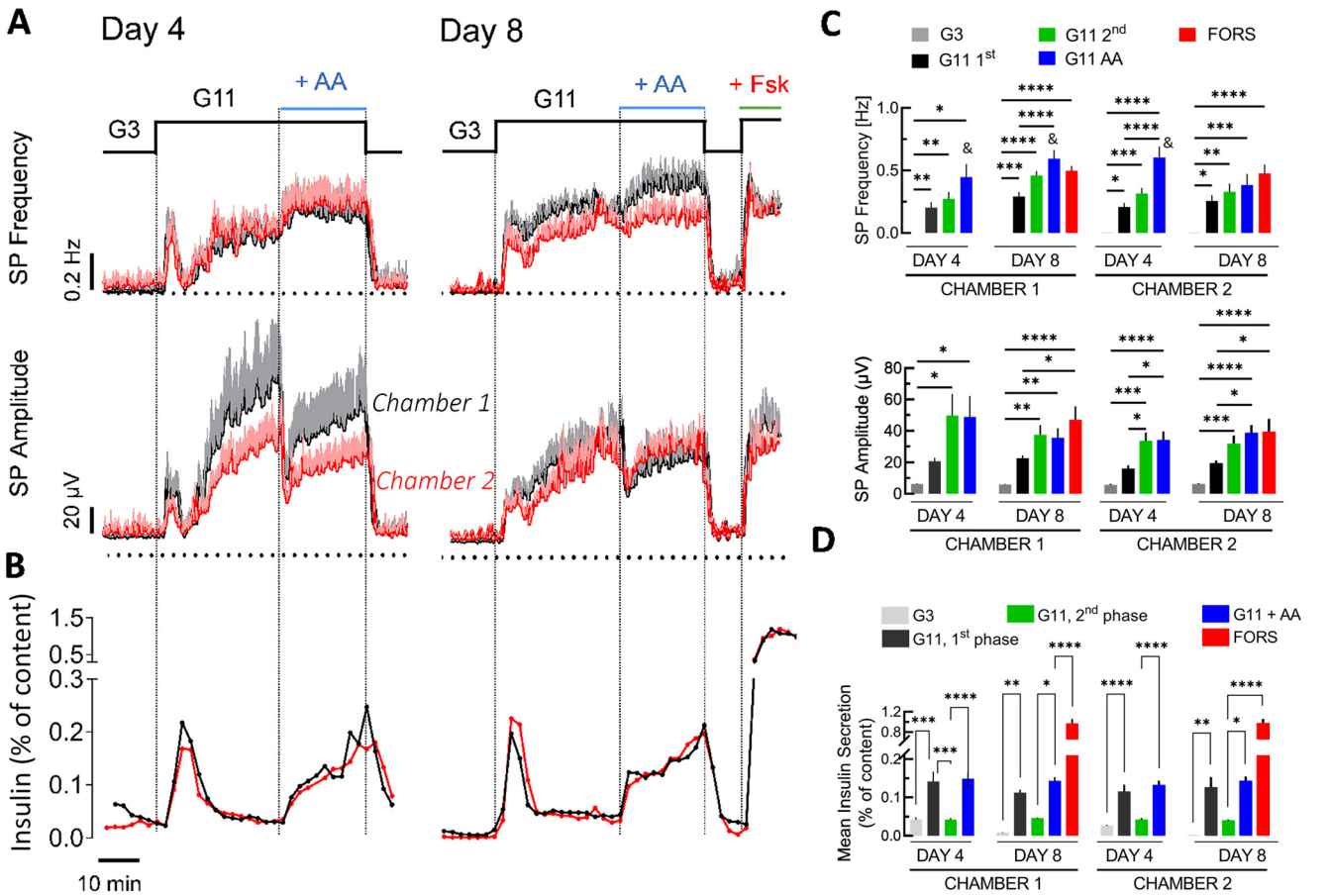

Fig. 5 Dynamic electrical and secretory β-cell activity after 4 and 8 days of culturing in the microfluidic MEA. (A) Stimulation of islet β-cell activity in response to glucose (3 or 11 mM) and amino acids (AA, 10 mM, in the presence of 11 mM glucose). Forskolin was only added at the end of recording on day 8. Black lines, chamber 1, red lines, chamber 2, given are means ± SEM, n = 22. SEM is given in grey or light red. (B) Insulin secretion (as percent of content; black, chamber 1, red, chamber 2; 162 islets/chamber). (C) Statistics of mean electrical activity (frequency, amplitude) for 3 mM glucose, 11 mM glucose (G11 1st phase or G11 2nd phase), 11 mM glucose and amino acids (G11 AA) or forskolin (10 µM). (D) Statistics of mean insulin secretion during perfusion with media as in (C). *, **, ***, ****, $2p < 0.05$, 0.01, 0.001 or 0.0001; &, $2p < 0.05$ *vs.* 2nd phase glucose alone (ANOVA/Tukey).

The kinetics of glucose concentration observed in our system were in the same range as those reported for other devices[52,53] and are also in line with those observed *in vivo* in mice upon glucose injection[54] and are clearly more physiological than square pulses of glucose, as used in static incubation. In addition, microfluidic flow has been shown to increase the penetration and speed of buffer exchange within the islet micro-organ.[53]

Applications of microfluidic devices have so far been limited mostly to short-term (≤48 h) islet assessments, including dynamic glucose-stimulated insulin secretion or calcium-based imaging[8,19,20,52,55,56] with only a few long-term applications.[10,12,57,58] In contrast to intracellular electrophysiological and calcium imaging, extracellular electrophysiology, as implemented here, is non-invasive and can be used in the long term or reused several days later to test conditions on the same preparation without exogenous probes or transgene expression.[59] The culture on the chip seems to improve survival in comparison with suspension cultures, as previously observed by others.[60,61]

A number of published devices for islets are designed for the investigation of single islets.[8,10,13,19] Although this provides high resolution, it may not always provide the best solution in view of the considerable heterogeneity of human and murine islets.[33,62] They also seem preferentially to trap larger islets,[8,19,44] which are not representative of the entire islet population.[33,62,63] This issue may be solved using dams or traps of different heights.[9,11,64,65] However, single-islet trapping devices have not been used in long-term investigations and these configurations would also complicate the alignment of the PDMS mask with electrodes.

Our device has limitations in terms of throughput, and comparability between chambers. In contrast to biochemical or imaging approaches, throughput remains limited, although considerably higher than with a classical perforated patch clamp. Nevertheless, the electrophysiological approach used here permits high-resolution kinetic analysis of the entire micro-organ activity and its coupling without resorting to complex *post hoc* algorithms.[7,34,36] Imaging is now possible in the kHz or near-kHz range, but only in a single optical

plane or as a line scan excluding capture of the whole micro-organ.[11,66,67] Note that MEA-based approaches have already proved useful for addressing a number of biological questions.[7,46,47,68,69]

The dual-chamber system allows concomitant comparisons and only one other dual-chamber design has been reported previously, but the performance of the chambers had not been compared.[70] In our device, SP frequencies remained comparable between the two chambers during the different experiments. In contrast, we noted in one set of experiments (Fig. 5A) a discrepancy in SP amplitude between the two chambers on day 4 of culturing. In contrast to frequency, extracellular recording of amplitude in these electrically coupled micro-organs depends on electrode coverage and may vary depending on adhesion or whether a single islet of less than 100 μm in diameter adheres and partially or completely covers an electrode with a diameter of 30 μm. Interestingly the difference between chambers was no longer apparent on day 8 of culturing. Therefore, sufficient culture time may be needed for uniform adhesion. Alternatively, normalisation of amplitude values, as shown here, may allow a comparison of kinetics between chambers. The loss of information on absolute values is acceptable as, in contrast to intracellular recordings (patch clamps), extracellularly recorded amplitudes do not represent absolute values. We have previously reported electrophoretic migration of islet cells to electrodes to ensure optimal coverage and their subsequent re-aggregation to pseudo-islets.[71] Such an approach may also be used to obtain more homogenous electrode–islet coupling in both chambers.

Another current limitation is given by the off-line nature of secretion measurement. Several elegant on-line read-outs for hormone measurements have been published[17,44,72,73] with a resolution of 0.1 Hz or less.[19,74] They provide very important information at high time resolution, but such approaches may not be feasible for most laboratories.

5. Conclusions

Analysis of islets in well-characterized electrophysiological microfluidic devices offers a number of advantages and perspectives. The ease of fabrication, assembly and handling should allow long-term on-line monitoring of islet activity in native micro-organs, pseudo-islets or stem-cell-derived islet-like organoids.[25,47,75] Future developments may include the controlled formation of islet cell spheroids, from native or stem-cell derived islet cells *via* application of an electric field directly on the electrode, thus circumventing complex islet trapping.[71] The use of electrochemical organic transistors provides high resolution and, in addition, the detection of single action potentials.[31] Sophisticated three-dimensional electrodes or even electrode meshes[76,77] may provide 3D electrophysiology of islets while retaining the high temporal resolution. Finally, electrodes and transistors may be manufactured for the recognition of specific ions, such as K^+ or Zn^{2+},[39,78] thus further advancing the analysis of islet function.

Data availability

The data that support the findings of this study are available from the corresponding author upon reasonable request.

Author contributions

ML: conceptualization, formal analysis, investigation, methodology, visualization, data curation, writing – original draft, writing – review & editing. LO: methodology, visualization. JG: methodology, investigation. KM: methodology, visualization. MM: methodology, visualization. AP: methodology. DC: methodology, investigation. EP: conceptualization, methodology. SR: supervision, writing – review & editing. MR: methodology, supervision writing – review & editing. JL: conceptualization, formal analysis, methodology, visualization, data curation, writing – original draft, writing – review & editing; funding acquisition.

Conflicts of interest

None.

Acknowledgements

This research has been supported by the French Ministry of Research *via* an excellence doctoral grant to ML and the French Research Agency ANR (ANR-21-CE14-0078 to JL and SR).

References

1 G. D. Collaborators, *Lancet*, 2023, **402**, 203–234.
2 M. A. Charles and R. D. Leslie, *Diabetes*, 2021, **70**, 2444–2456.
3 R. Regeenes and J. V. Rocheleau, *Lab Chip*, 2024, **24**, 1327–1350.
4 M. P. Dybala, J. K. Butterfield, B. K. Hendren-Santiago and M. Hara, *Diabetes*, 2020, **69**, 1864–1874.
5 P. Rorsman and F. M. Ashcroft, *Physiol. Rev.*, 2018, **98**, 117–214.
6 J. E. Campbell and C. B. Newgard, *Nat. Rev. Mol. Cell Biol.*, 2021, **22**, 142–158.
7 M. Jaffredo, E. Bertin, A. Pirog, E. Puginier, J. Gaitan, S. Oucherif, F. Lebreton, D. Bosco, B. Catargi, D. Cattaert, S. Renaud, J. Lang and M. Raoux, *Diabetes*, 2021, **70**, 878–888.
8 M. Nourmohammadzadeh, Y. Xing, J. W. Lee, M. A. Bochenek, J. E. Mendoza-Elias, J. J. McGarrigle, E. Marchese, Y. Chun-Chieh, D. T. Eddington, J. Oberholzer and Y. Wang, *Lab Chip*, 2016, **16**, 1466–1472.
9 R. Perrier, A. Pirog, M. Jaffredo, J. Gaitan, B. Catargi, S. Renaud, M. Raoux and J. Lang, *Biosens. Bioelectron.*, 2018, **117**, 253–259.
10 Y. Jun, J. Lee, S. Choi, J. H. Yang, M. Sander, S. Chung and S. H. Lee, *Sci. Adv.*, 2019, **5**, eaax4520.
11 H. Ren, Y. Li, C. Han, Y. Yu, B. Shi, X. Peng, T. Zhang, S. Wu, X. Yang, S. Kim, L. Chen and C. Tang, *Nat. Commun.*, 2022, **13**, 3721.

12 P. Sokolowska, K. Zukowski, J. Janikiewicz, E. Jastrzebska, A. Dobrzyn and Z. Brzozka, *Biosens. Bioelectron.*, 2021, **183**, 113215.
13 T. Tao, P. Deng, Y. Wang, X. Zhang, Y. Guo, W. Chen and J. Qin, *Adv. Sci.*, 2022, **9**, e2103495.
14 R. Zandi Shafagh, S. Youhanna, J. Keulen, J. X. Shen, N. Taebnia, L. C. Preiss, K. Klein, F. A. Buttner, M. Bergqvist, W. van der Wijngaart and V. M. Lauschke, *Adv. Sci.*, 2022, **9**, e2203368.
15 Y. Nashimoto, A. Konno, T. Imaizumi, K. Nishikawa, K. Ino, T. Hori, H. Kaji, H. Shintaku, M. Goto and H. Shiku, *Biotechnol. Bioeng.*, 2024, **121**, 1050–1059.
16 C. Quintard, E. Tubbs, G. Jonsson, J. Jiao, J. Wang, N. Werschler, C. Laporte, A. Pitaval, T. S. Bah, G. Pomeranz, C. Bissardon, J. Kaal, A. Leopoldi, D. A. Long, P. Blandin, J. L. Achard, C. Battail, A. Hagelkruys, F. Navarro, Y. Fouillet, J. M. Penninger and X. Gidrol, *Nat. Commun.*, 2024, **15**, 1452.
17 M. G. Roper, J. G. Shackman, G. M. Dahlgren and R. T. Kennedy, *Anal. Chem.*, 2003, **75**, 4711–4717.
18 A. M. Schrell, N. Mukhitov, L. Yi, J. E. Adablah, J. Menezes and M. G. Roper, *Anal. Methods*, 2017, **9**, 38–45.
19 Y. Wang, R. Regeenes, M. Memon and J. V. Rocheleau, *Cells Rep. Methods*, 2023, **3**, 100602.
20 N. Bruce, I. A. Wei, W. Leng, Y. Oh, Y. C. Chiu, M. G. Roper and R. Bertram, *Am. J. Physiol.*, 2022, **323**, E492–E502.
21 J. V. Rocheleau, G. M. Walker, W. S. Head, O. P. McGuinness and D. W. Piston, *Proc. Natl. Acad. Sci. U. S. A.*, 2004, **101**, 12899–12903.
22 J. T. Walker, R. Haliyur, H. A. Nelson, M. Ishahak, G. Poffenberger, R. Aramandla, C. Reihsmann, J. R. Luchsinger, D. C. Saunders, P. Wang, A. Garcia-Ocana, R. Bottino, A. Agarwal, A. C. Powers and M. Brissova, *JCI Insight*, 2020, **5**, e137017.
23 J. J. Davis, M. J. Donohue, E. O. Ogunkunle, W. J. Eaton, D. J. Steyer and M. G. Roper, *Anal. Bioanal. Chem.*, 2023, **415**, 5671–5680.
24 W. J. Eaton and M. G. Roper, *Anal. Methods*, 2021, **13**, 3614–3619.
25 A. L. Glieberman, B. D. Pope, D. A. Melton and K. K. Parker, *Diabetes*, 2021, **70**, 347–363.
26 M. E. Obien, K. Deligkaris, T. Bullmann, D. J. Bakkum and U. Frey, *Front. Neurosci.*, 2014, **8**, 423.
27 L. Xu, C. Hu, Q. Huang, K. Jin, P. Zhao, D. Wang, W. Hou, L. Dong, S. Hu and H. Ma, *Biosens. Bioelectron.*, 2021, **175**, 112854.
28 F. J. Iniguez-Lomeli, Y. Bornat, S. Renaud, J. H. Barron-Zambrano and H. Rostro-Gonzalez, *Neural. Comput. Appl.*, 2021, **33**, 12121–12140.
29 J. Park, Z. Wu, P. R. Steiner, B. Zhu and J. X. J. Zhang, *Ann. Biomed. Eng.*, 2022, **50**, 111–137.
30 J. Wan, S. Zhou, H. J. Mea, Y. Guo, H. Ku and B. M. Urbina, *Chem. Rev.*, 2022, **122**, 7142–7181.
31 M. Abarkan, A. Pirog, D. Mafilaza, G. Pathak, G. N'Kaoua, E. Puginier, R. O'Connor, M. Raoux, M. J. Donahue, S. Renaud and J. Lang, *Adv. Sci.*, 2022, **9**, e2105211.
32 E. Puginier, K. Leal-Fischer, J. Gaitan, M. Lallouet, P. A. Scotti, M. Raoux and J. Lang, *Front. Endocrinol.*, 2024, **15**, 1402880.
33 R. Arrojo e Drigo, Y. Ali, J. Diez, D. K. Srinivasan, P. O. Berggren and B. O. Boehm, *Diabetologia*, 2015, **58**, 2218–2228.
34 M. Raoux, Y. Bornat, A. Quotb, B. Catargi, S. Renaud and J. Lang, *J. Physiol.*, 2012, **590**, 1085–1091.
35 B. E. Peercy and D. J. Hodson, *eLife*, 2024, **13**, e95103.
36 F. Lebreton, A. Pirog, I. Belouah, D. Bosco, T. Berney, P. Meda, Y. Bornat, B. Catargi, S. Renaud, M. Raoux and J. Lang, *Diabetologia*, 2015, **58**, 1291–1299.
37 B. Thompson and L. S. Satin, *Compr. Physiol.*, 2021, **11**, 1–21.
38 C. J. Easley, J. V. Rocheleau, W. S. Head and D. W. Piston, *Anal. Chem.*, 2009, **81**, 9086–9095.
39 T. Nicolini, S. Shinde, R. El-Attar, G. Salinas, D. Thuau, M. Abbas, M. Raoux, J. Lang, E. Cloutet and A. Kuhn, *Adv. Mater. Interfaces*, 2024, **11**, 2400127.
40 E. L. Vanderlaan, J. K. Nolan, J. Sexton, C. Evans-Molina, H. Lee and S. L. Voytik-Harbin, *Biosens. Bioelectron.*, 2023, **235**, 115409.
41 X. J. Huang, A. M. O'Mahony and R. G. Compton, *Small*, 2009, **5**, 776–788.
42 D. J. Guckenberger, T. E. de Groot, A. M. D. Wan, D. J. Beebe and E. W. K. Young, *Lab Chip*, 2015, **15**, 2364–2378.
43 D. Kazmer, in *Applied Plastics Engineering Handbook*, ed. M. Kutz, William Andrew Publishing, 2nd edn, 2017, pp. 617–634.
44 A. L. Glieberman, B. D. Pope, J. F. Zimmerman, Q. Liu, J. P. Ferrier, J. H. R. Kenty, A. M. Schrell, N. Mukhitov, K. L. Shores, A. B. Tepole, D. A. Melton, M. G. Roper and K. K. Parker, *Lab Chip*, 2019, **19**, 2993–3010.
45 P. Buchwald, A. Tamayo-Garcia, V. Manzoli, A. A. Tomei and C. L. Stabler, *Biotechnol. Bioeng.*, 2018, **115**, 232–245.
46 M. Abarkan, J. Gaitan, F. Lebreton, R. Perrier, M. Jaffredo, C. Mulle, C. Magnan, M. Raoux and J. Lang, *Mol. Metab.*, 2019, **30**, 152–160.
47 M. Jaffredo, N. A. J. Krentz, B. Champon, C. E. Duff, S. Nawaz, N. Beer, C. Honore, A. Clark, P. Rorsman, J. Lang, A. L. Gloyn, M. Raoux and B. Hastoy, *Diabetes*, 2024, **73**, 1255–1265.
48 L. Zhu, D. Dattaroy, J. Pham, L. Wang, L. F. Barella, Y. Cui, K. J. Wilkins, B. L. Roth, U. Hochgeschwender, F. M. Matschinsky, K. H. Kaestner, N. M. Doliba and J. Wess, *JCI Insight*, 2019, **5**, e127994.
49 M. Nourmohammadzadeh, J. F. Lo, M. Bochenek, J. E. Mendoza-Elias, Q. Wang, Z. Li, L. Zeng, M. Qi, D. T. Eddington, J. Oberholzer and Y. Wang, *Anal. Chem.*, 2013, **85**, 11240–11249.
50 T. Ang, C. R. Bruce and G. M. Kowalski, *Diabetes*, 2019, **68**, 939–946.
51 M. E. Capozzi, B. Svendsen, S. E. Encisco, S. L. Lewandowski, M. D. Martin, H. Lin, J. L. Jaffe, R. W. Coch, J. M. Haldeman, P. E. MacDonald, M. J. Merrins, D. A. D'Alessio and J. E. Campbell, *JCI Insight*, 2019, **4**, e126742.
52 X. Li, J. C. Brooks, J. Hu, K. I. Ford and C. J. Easley, *Lab Chip*, 2017, **17**, 341–349.
53 K. S. Sankar, B. J. Green, A. R. Crocker, J. E. Verity, S. M. Altamentova and J. V. Rocheleau, *PLoS One*, 2011, **6**, e24904.

54 C. Thibault, C. Guettet, M. C. Laury, J. M. N'Guyen, M. A. Tormo, D. Bailbé, B. Portha, L. Pénicaud and A. Ktorza, *Diabetologia*, 1993, **36**, 589–595.
55 P. Wu Jin, N. Rousset, A. Hierlemann and P. M. Misun, *Front. Bioeng. Biotechnol.*, 2021, **9**, 674431.
56 P. M. Misun, B. Yesildag, F. Forschler, A. Neelakandhan, N. Rousset, A. Biernath, A. Hierlemann and O. Frey, *Adv. Biosyst.*, 2020, **4**, e1900291.
57 I. Goswami, E. de Klerk, P. Carnese, M. Hebrok and K. E. Healy, *Lab Chip*, 2022, **22**, 4430–4442.
58 K. Schlünder, M. Cipriano, A. Zbinden, S. Fuchs, T. Mayr, K. Schenke-Layland and P. Loskill, *Lab Chip*, 2024, **24**, 2080–2093.
59 S. Fleischer, H. G. Jahnke, E. Fritsche, M. Girard and A. A. Robitzki, *Biosens. Bioelectron.*, 2019, **126**, 624–631.
60 H. Liu, Y. Wang, H. Wang, M. Zhao, T. Tao, X. Zhang and J. Qin, *Adv. Sci.*, 2020, **7**, 1903739.
61 E. L. Vanderlaan, J. Sexton, C. Evans-Molina, A. Buganza Tepole and S. L. Voytik-Harbin, *Lab Chip*, 2023, **23**, 4466–4482.
62 M. P. Dybala and M. Hara, *Diabetes*, 2019, **68**, 1230–1239.
63 A. Kim, K. Miller, J. Jo, G. Kilimnik, P. Wojcik and M. Hara, *Islets*, 2009, **1**, 129–136.
64 K. S. Sankar, S. M. Altamentova and J. V. Rocheleau, *PLoS One*, 2019, **14**, e0222424.
65 R. Regeenes, Y. Wang, A. Piro, A. Au, C. M. Yip, M. B. Wheeler and J. V. Rocheleau, *Biosens. Bioelectron.: X*, 2023, **13**, 100285.
66 E. Jin, J. K. Briggs, R. K. P. Benninger and M. J. Merrins, *bioRxiv*, 2024, preprint, DOI: **10.1101/2024.08.21.608680**.
67 J. Dolenšek, V. Pohorec, M. Skelin Klemen, M. Gosak and A. Stožer, *Acta Physiol.*, 2025, **241**, e14261.
68 M. Raoux, P. Vacher, J. Papin, A. Picard, E. Kostrzewa, A. Devin, J. Gaitan, I. Limon, M. J. Kas, C. Magnan and J. Lang, *Diabetologia*, 2015, **58**, 749–757.
69 M. Raoux, S. Lablanche, M. Jaffredo, A. Pirog, P. Y. Benhamou, F. Lebreton, A. Wojtusciszyn, D. Bosco, T. Berney, S. Renaud, J. Lang and B. Catargi, *Transplant Int.*, 2023, **36**, 11512.
70 D. Lee, Y. Wang, J. E. Mendoza-Elias, A. F. Adewola, T. A. Harvat, K. Kinzer, D. Gutierrez, M. Qi, D. T. Eddington and J. Oberholzer, *Biomed. Microdevices*, 2012, **14**, 7–16.
71 E. Pedraza, A. Karajic, M. Raoux, R. Perrier, A. Pirog, F. Lebreton, S. Arbault, J. Gaitan, S. Renaud, A. Kuhn and J. Lang, *Lab Chip*, 2015, **15**, 3880–3890.
72 A. M. Schrell, N. Mukhitov, L. Yi, J. E. Adablah, J. Menezes and M. G. Roper, *Anal. Methods*, 2017, **9**, 38–45.
73 M. Yang, K. Mandal, M. Södergren, Ö. Dumral, L. Winroth and A. Tengholm, *Acta Physiol.*, 2025, **241**, e14268.
74 J. E. Adablah, Y. Wang, M. Donohue and M. G. Roper, *Anal. Chem.*, 2020, **92**, 8464–8471.
75 M. S. H. Friedlander, V. M. Nguyen, S. K. Kim and R. J. Bevacqua, *Diabetes*, 2021, **70**, 1051–1060.
76 H. Yuk, B. Lu, S. Lin, K. Qu, J. Xu, J. Luo and X. Zhao, *Nat. Commun.*, 2020, **11**, 1604.
77 Q. Li, K. Nan, P. Le Floch, Z. Lin, H. Sheng, T. S. Blum and J. Liu, *Nano Lett.*, 2019, **19**, 5781–5789.
78 A. Villarroel Marquez, G. Salinas, M. Abarkan, M. Idir, C. Brochon, G. Hadziioannou, M. Raoux, A. Kuhn, J. Lang and E. Cloutet, *Macromol. Rapid Commun.*, 2020, **41**, e2000134.